AIAA JOURNAL
Vol. 34, No. 5, May 1996

Experimental and Numerical Investigations of Dynamic Stall on a Pitching Airfoil

Philippe Wernert*
ISL, French-German Research Institute of Saint-Louis, F-68300 Saint-Louis, France
and
Wolfgang Geissler,† Markus Raffel,† and Jürgen Kompenhans†
DLR, German Aerospace Research Establishment, D-37073 Göttingen, Germany

The dynamic stall process on a pitching NACA 0012 airfoil was investigated by two experimental techniques—particle image velocimetry (PIV) and laser-sheet visualizations—and a numerical code based on the Navier–Stokes equations. The freestream velocity was 28 m/s, leading to a Reynolds number (based on airfoil chord) of 3.73×10^5. The airfoil motion was a sinusoidal function between 5 and 25 deg of incidence, with a frequency of 6.67 Hz corresponding to a reduced frequency (based on airfoil half-chord) of 0.15. The out-of-plane component of the vorticity could be derived from the PIV velocity fields. The comparison between experimental and numerical results was conducted for the four main phases of the dynamic stall process, i.e., attached flow, development of the dynamic stall vortex, poststall vortex shedding, and reattachment. In general, the computational results agreed very well with the experimental results. However, some discrepancies were observed and discussed. The cycle-to-cycle nonreproducibility of the flowfield during the phase of massive separation is also mentioned.

Introduction

DYNAMIC stall is a term that is often used to describe the complex series of events that happen when an airfoil is put in motion to incidences beyond the static stall angle. The evolution of the flowfield is rather different from that obtained for static stall, because many dynamic effects are involved. This phenomenon can appear in a variety of situations (e.g., helicopter rotor blades, rapidly maneuvering aircraft, or turbomachinery cascades) and is the source of both desirable or undesirable effects.

Kramer,[1] in 1932, first recognized the dynamic features associated with the rapid variations of incidence experienced by an airfoil. After this early investigation, these dynamic effects received little attention by aerodynamicists until they were identified on helicopter blades during the 1960s. These investigations were initiated to better understand the stall flutter problem, which occurs on the retreating blades because of high incidences and separated flow. Moreover, because the overall performance of a rotor is limited by the stall risk on retreating blades, dynamic stall is an important problem to be studied.

Major progress was accomplished after it was shown that the dynamic stall process on a blade is associated with the formation, development, and shedding of a strong vortex structure on the blade upperside and that this configuration can be reproduced on a pitching airfoil in a two-dimensional flow. Since then, many experiments have been conducted on pitching airfoils, to document the dynamic stall process for different test conditions: The effects of freestream Mach number, airfoil geometry, and airfoil motions have been investigated in detail.[2] In most cases, sinusoidal pitching motions have been considered because these functions are close to the incidence variations experienced by a real rotor blade.

Most of these experiments have been realized by use of pressure transducers, flow visualization methods, and hot wires. These techniques have provided a great amount of data concerning the pressure distribution on the airfoil upperside (and calculation of lift, drag, and pitching moment), the dynamic stall vortex (convection speed, chordwise location, spatial extent, shedding process), and the unsteady boundary layer (displacements of the laminar–turbulent transition, flow reversal, and separation points).

A variety of numerical methods have been applied to the dynamic stall problem. On the basis of coupling procedures between unsteady boundary layers and outer inviscid flows, it was possible to extend the calculation into regions where the flow is reversed.[3] But without flow modeling, the calculation ended at dynamic stall onset. Thus, the start and formation of the dynamic stall vortex could not be treated in this way. Mehta[4] obtained first results on an oscillating airfoil using the complete set of unsteady Navier–Stokes equations for laminar flows. With the addition of suitable turbulence models, the problem of unsteady high-Reynolds-number flows could be treated successfully using different concepts for the numerical treatment of the flow.[5]

All of these experimental, theoretical, and numerical results have led to a detailed knowledge of the main features of the flowfield over a pitching airfoil in dynamic stall conditions. Many reviews concerning these results have been published.[6] To improve our knowledge of the dynamic stall process and to have a more accurate data basis for the validation of new numerical methods, it is now essential to examine in detail the velocity flowfield on the upperside of the airfoil. Until very recently, only one nonintrusive technique for measuring the velocity in a complex flowfield was available: laser Doppler anemometry (LDA). This technique has been used widely in many domains of fluid mechanics and aerodynamics and is particularly useful for steady flow because of its pointwise character. In the case of an unsteady flow, the reconstruction of complete flowfields is possible if a periodicity appears: the method of conditional sampling (or ensemble averaging) then can be used.[7] In this way, the LDA technique has been applied to the dynamic stall problem (the required periodicity is given by the airfoil motion) and has revealed strong unsteady processes in the flow.[8] To have a better general view of the real evolution and aperiodic features of such a velocity flowfield, it is necessary to use an instantaneous and global (not pointwise) source of information. Such global techniques have been developed during the past years.

To study the velocity flowfield over a sinusoidal pitching airfoil operating under dynamic stall conditions, the most useful technique, i.e., particle image velocimetry (PIV),[9,10] was chosen in the present investigations. The experimental data obtained by the PIV method were completed with laser-sheet visualizations and numerical calculations, to gain a detailed point of view of the dynamic-stall flow phenomena.

Received Dec. 27, 1994; revision received Oct. 15, 1995; accepted for publication Jan. 5, 1996.

*Research Scientist, Department of Aerodynamics.
†Research Scientist, Institute for Fluid Mechanics.

Experimental Facility

Wind Tunnel and Airfoil

The experiments were conducted in the Institute of Saint Louis (ISL) low-speed wind tunnel. This tunnel has an open, rectangular test section 70 cm wide, 80 cm long, and 90 cm high. The freestream turbulence is less than 0.25%.

The chosen airfoil had a NACA 0012 cross section of $c = 20$-cm chord and 56-cm span. It was mounted between two circular end plates of Plexiglas® (40-cm diam) to ensure a two-dimensional flow in the vertical center plane of the test section. The airfoil oscillated around an axis located at 25% chord from the leading edge.

Driving Mechanism

The airfoil motion to be investigated is provided by a novel system[11,12] that includes a user-programmable control unit, two variable-speed drives, each controlling a brushless motor (this system has been designed to produce pitching and heaving motions), and a support system, essentially adapted to transmit the motions from the motors to the airfoil. The airfoil motions are programmed on the basis of a point-by-point procedure that allows a large domain of motions to be investigated. Thus, it is possible to obtain periodic motions (harmonic, sawtooth, or more complex motions) or transient motions (steps, ramps) with a maximum frequency of 15 Hz for pitching motions and 7 Hz for heaving motions.

Laser-Sheet Visualizations

The laser sheet is generated by a continuous argon laser (3–4 W), mirrors to lead the laser beam to the top of the wind tunnel test section, and a cylindrical and a converging lens, which expand the beam into a vertical plane about 1 mm thick, located at airfoil midspan (Fig. 1). Vaporized oil particles were injected in the flow, about 20 cm upstream from the airfoil leading edge. The airfoil was painted black to avoid light reflections. White marks were drawn on the airfoil suction side (at midspan) to estimate the chordwise location of the vortex structures easily.

Pictures were taken with a video camera (Sony TR-808) operating at the standard frequency of 25 pictures per second. One important parameter to be defined was the camera shutter speed. A compromise had to be found between a high shutter speed (i.e., a short recording time) to freeze the vortex development on the pictures and a low shutter speed (i.e., a longer recording time) to have enough light scattered by the seeding particles; 1 ms was chosen.

A display system showing the instantaneous incidence of the airfoil measured by an incremental rotary encoder was mounted near the airfoil, in the observation field of the camera. A synchronization system based on the camera output video signal was developed to freeze the incidence value displayed at exactly the instant when the charge-coupled device (CCD) sensor of the camera begins to record the picture. This system allowed us to know the instantaneous incidence of the airfoil for each picture with an accuracy of 0.01 deg.[13]

The recorded pictures were then digitized, and image processing techniques were employed for two purposes: 1) to improve the contrast of the pictures by using spatial filters and 2) to rearrange them to obtain a video movie.

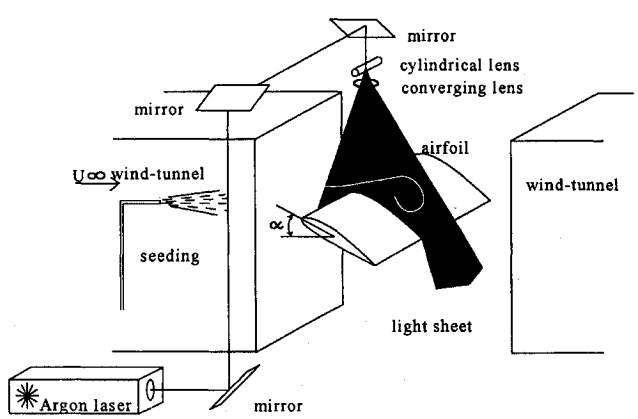

Fig. 1 Wind-tunnel geometry and experimental setup for flow visualizations.

PIV System

The PIV system[12] developed at DLR is composed of a double-oscillator Nd:YAG pulse laser with an output energy of 70 mJ for each pulse and a typical time delay between the two pulses of about 12 μs, a photographic recording system with a 2.8 β-number objective and Kodak TMAX 3200 recording material, several Laskin nozzle atomizers in parallel, and a specially developed low-disturbance injection device to seed the flow with olivè oil droplets of about 1-μm mean diameter.[14]

To save time when aligning the system, the 35-mm camera was equipped with a fast-focusing device composed of a carefully aligned CCD sensor mounted in its viewfinder. A high-speed rotating mirror system[15] was used as an image shifting system for the determination of reverse-flow regions and the adaptation of the measured velocity range to the range of optimal evaluation.

The evaluation of the photographic PIV recordings was performed by means of the standard analog–optical/digital method, i.e., by means of the digital fast Fourier transform of Young's fringes pattern. Typically, approximately 3000 instantaneous velocity vectors were determined for each PIV recording. A validation algorithm[16] was then used to eliminate some erroneously determined velocity vectors. It should be emphasized that for all PIV results presented in this paper, only this validation algorithm was applied; no smoothing (e.g., by means of Gaussian filters) or interpolation of missing data was carried out.

The PIV recordings were taken during the upstroke and the downstroke motions of the model in intervals of 1 deg and at a rate of about one picture per second. By means of a high-precision pulse generator, 6 PIV pictures could be recorded for each airfoil incidence at exactly the same phase of the pitching motion (with each picture being taken out of a different cycle).

This PIV system was able to resolve vortex structures in flows with turbulence levels lower than 0.6%.[14]

Numerical Investigations

The solution process of the unsteady two-dimensional Navier–Stokes equations is based on the approximate-factorization implicit method originally developed by Beam and Warming.[17] This method is working in a curvilinear-airfoil-fitted coordinate system. The coordinates are allowed to deform with respect to time, meshlines are fixed to the airfoil and to the outer boundary. These boundaries are at a large distance (about 10 chords) from the airfoil to avoid reflections; a vortex correction is also made there. Extremely fine mesh spacings adjacent to the airfoil surface were implemented to resolve the turbulent boundary layer sufficiently. The extension to curvilinear coordinates and the solution of the transformed system are described by Geissler.[18] The calculations have been carried out by using the simple Baldwin–Lomax algebraic turbulence model[19] and assuming the occurrence of a fully turbulent flow on the airfoil. This assumption is made because of a lack of information about the time-dependent location of the laminar–turbulent transition point. The consequences of this assumption are discussed in the Discussion section. Details about the numerical code can be found in Refs. 3, 5, 18, 20, and 21.

Results

Airfoil Motion

The selected airfoil motion had the following incidence law:

$$\alpha(t) = 15\,\text{deg} + 10\,\text{deg}\sin(2\pi f t) \tag{1}$$

with a frequency $f = 6.67$ Hz. The freestream velocity was $U_\infty = 28$ m/s, corresponding to a Reynolds number, based on chord length, of 3.73×10^5. These values led to a reduced frequency (referred to half chord) of

$$\Omega = 2\pi f c/2U_\infty = 0.15 \tag{2}$$

The incidence variation of ±10 deg, the mean incidence of 15 deg, and the above-mentioned value of reduced frequency correspond to the deep-stall case according to the description given by McCroskey.[6] Strong unsteady effects thus can be expected. Further experimental and numerical investigations have been carried out by other researchers for the same conditions: same airfoil, incidence law, and reduced frequency, but with different wind-tunnel configuration and Reynolds number.[2,22,23] Hence, these investigations provide a good data basis for the comparison with our results.

Presentation of the Results

To follow the evolution of the dynamic stall process in a relevant way, the three types of results obtained, i.e., PIV data, visualization pictures, and numerical data, are now presented at the same stage of flow development for increasing phases of the airfoil motion. Both the experimental and the numerical data are available as velocity vector plots for a large number of angles of attack or time steps. From this huge amount of data, only a few pictures concerning the four main events of the investigated flowfield, i.e., existence of attached flow, development of the dynamic stall vortex, post-stall vortex shedding, and reattachment process, have been selected and are shown. These selected pictures are typical of the kinds of flowfields encountered.

For a clear interpretation of the results, the vector fields were first integrated, yielding instantaneous streamlines for both calculated and measured data fields. The number of streamlines was limited to make the numerical data more comparable to the PIV results. The experimentally determined PIV velocity vector field also is included in these plots.

These streamlines then can be compared to the streaklines seen on the visualization pictures. The incidences of the airfoil at the instants when the CCD camera starts and stops the recording are given in the captions.

One important quantity necessary for the interpretation of unsteady separated flowfields is vorticity. In both experimental and numerical cases, the out-of-plane vorticity field ω_z has been numerically derived from the two-dimensional velocity field and normalized, yielding the following quantity:

$$\tilde{\omega}_z = \omega_z c / U_\infty \tag{3}$$

The experimental and numerical vorticity fields are also shown for each of the four main events considered. On these pictures, the vorticity isolines step is $\Delta\tilde{\omega}_z = 6.67$.

Attached Flow, α = 15-deg Upstroke

Figure 2a shows both the experimental and the numerical streamlines corresponding to the incidence of 15 deg during upstroke. The flowfield is seen to be attached in both cases. Deviations between experimental and numerical results are observed when comparing the directions of the streamlines: for the same incidence of 15-deg upstroke, the streamlines deduced from PIV measurements are more inclined than the streamlines deduced from calculations, i.e., the measured flowfield is at a more advanced stage of flow development than the numerical one. Because the flow conditions for measurements and calculations are exactly the same, the observed deviations in streamline directions could be due (at least in part) to wind tunnel effects.[24] However, no satisfying theory is available for unsteady attached or separated flowfields, and so, no incidence correction has been estimated. Figure 2b shows a visualization picture corresponding to the same stage of flow development as in Figure 2a: The flow is also seen to be attached, although a thin layer without particles can be recognized on the airfoil upperside. Indeed, it is well known that the classic criterion for steady separation (vanishing of the skin friction coefficient at the wall) is no longer valid in unsteady flow. Instead, the point of zero skin friction oscillates along the airfoil surface, generating a thin layer of reverse flow with separation occurring at some downstream location.[25] In their classic description of the dynamic stall process on a pitching NACA 0012 airfoil at high Reynolds number, Carr et al.[2] identified the rapid upstream motion of the thin reverse-flow layer from the trailing edge as one of the major events preceding the formation of the dynamic stall vortex at the leading edge. By use of a slanted rotating hot wire on a NACA 0012 airfoil pitching at a Reynolds number of 3×10^5, De Ruyck et al.[26] reached a similar conclusion. Numerical evidence of the existence of such a thin reverse-flow layer also is given by Geissler et al.[3,20] In Ref. 20, it is shown that the fluid elements composing this reverse-flow layer are coming from the airfoil pressure side before moving around the trailing edge. Because in the present visualization investigations the airfoil pressure side was not seeded, the occurrence of the thin reverse-flow layer in Fig. 2b is consistent with the results found in the literature. Because the flow is attached, no vortex structure is involved at this time of flow development. Consequently, the experimental and numerical vorticity fields are not shown.

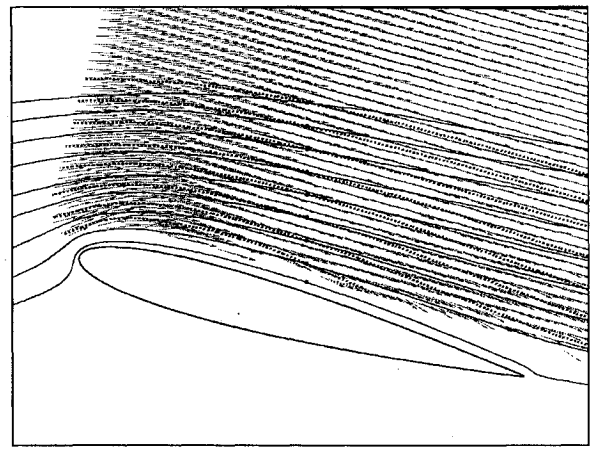

a) - - - -, PIV, α = 15 deg up and ——, calculations, α = 15 deg up

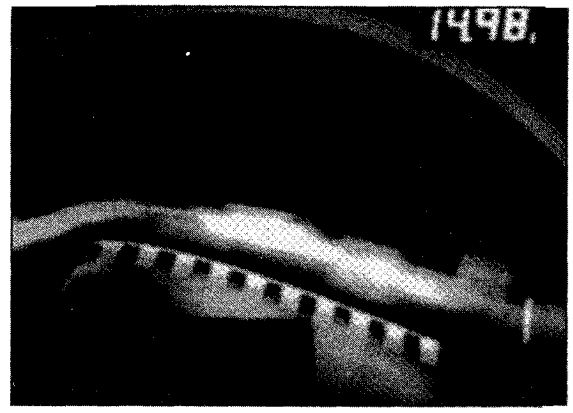

b) 14.98 deg < α < 15.39 deg

Fig. 2 Phase of attached flow (upstroke motion): a) PIV velocity vector field and streamlines from calculations and PIV experiment and b) visualization picture.

Development of the Dynamic Stall Vortex, $\alpha \geq$ 22-deg Upstroke

The next series of figures shows three instantaneous streamline plots (Figs. 3a–3c) and the corresponding vorticity contours (Figs. 3d–3f) from the most interesting part of the oscillatory cycle. The flow is no longer attached, and a vortex structure is seen to develop on the airfoil upperside for both experimental and numerical results. The streamline plots of the numerical results were chosen in such a way that they show a vortex structure having the same spatial extension as the experimental ones have. For the reasons discussed above, the incidences of the selected numerical plots (α = 24, 24.3, and 24.7 deg) are different from the incidences of the experimental plots (α = 22, 23, and 24 deg). The vorticity plots then show a remarkable coincidence between calculated and measured vortex strengths and between calculated and measured locations of the vortex center.

However, the experimental streamlines and vorticity plots exhibit very fine structures that are absent in the numerical results.

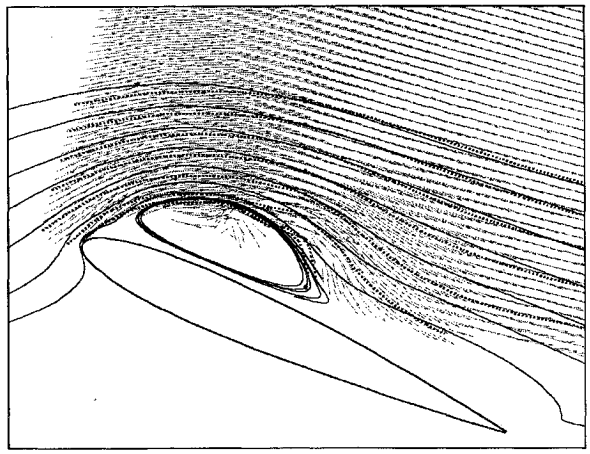

a) - - - -, PIV, α = 22 deg up and ——, calculations, α = 24 deg up

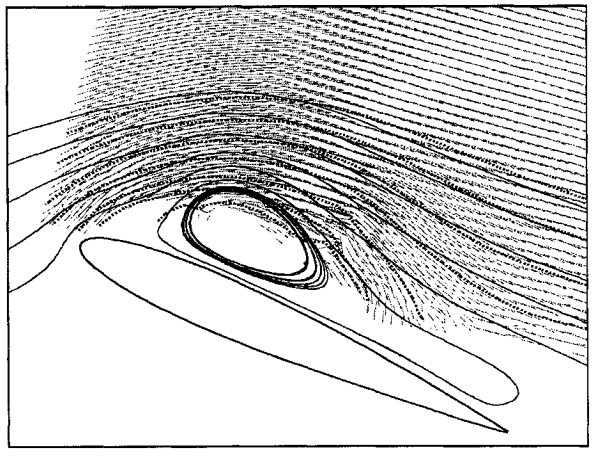

b) - - - -, PIV, α = 23 deg up and ——, calculations, α = 24.3 deg up

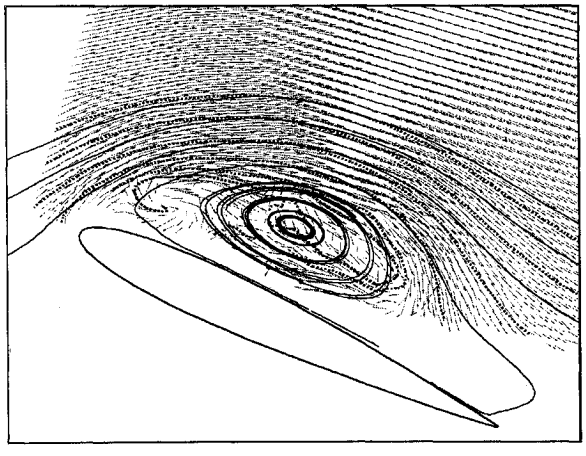

c) - - - -, PIV, α = 24 deg up and ——, calculations, α = 24.7 deg up

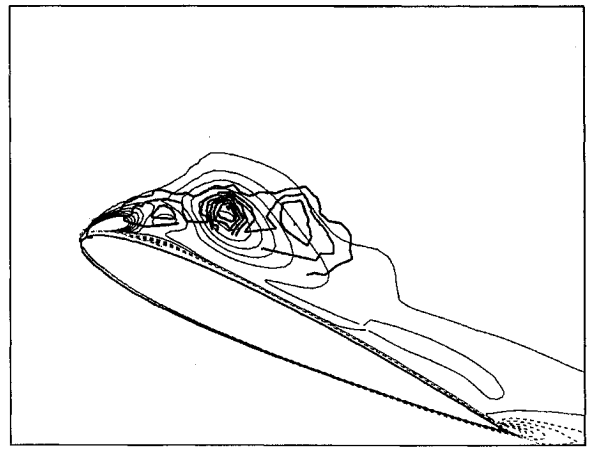

d) PIV. α = 22 deg up: ——, clockwise and - - - -, counterclockwise calculations; α = 24 deg up: ——, clockwise and – – –, counterclockwise

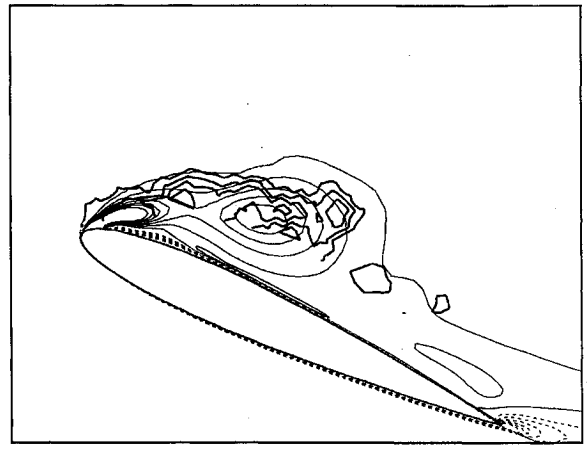

e) PIV. α = 23 deg up: ——, clockwise and - - - -, counterclockwise calculations; α = 24.3 deg up: ——, clockwise and – – –, counterclockwise

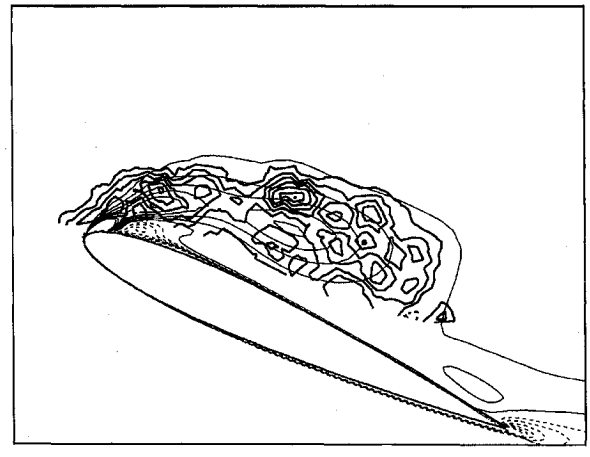

f) PIV. α = 24 deg up: ——, clockwise and - - - -, counterclockwise calculations; α = 24.7 deg up: ——, clockwise and – – –, counterclockwise

Fig. 3 Phase of development of dynamic stall vortex (upstroke motion): a–c) PIV velocity vector field and streamlines from calculations and PIV experiment and d–f) vorticity contours from calculations and PIV experiments.

Thus, small-scale vortices can be recognized on the PIV pictures even within the large dynamic stall vortex. Indeed, some scatter in the experimental vorticity plots may be attributed to the numerical operation of derivation of the measured velocity fields, whereas the absence of such structures in the results of calculations may be related to the use of the simple turbulence model.

A closer examination of the PIV pictures also shows a lack of velocity vectors in some critical flow regions: airfoil surface and leading and trailing edges. This can be explained mainly by the limitations of the experimental techniques and by the nonoptimal distribution of tracer particles, as explained in Ref. 12. Because these three flow areas are essential to the complete understanding of the dynamic stall process, further experimental improvements are required.

Figure 3g shows a visualization picture taken during the phase of development of the dynamic stall vortex. Comparison of this picture

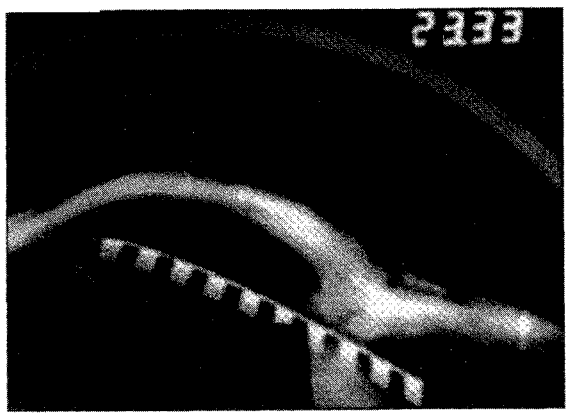

g)

Fig. 3 (Continued) Phase of development of dynamic stall vortex (upstroke motion): g) visualization picture: 23.33 deg < α < 23.55 deg.

with the streamline or vorticity plots indicates that the streaklines obtained by laser-sheet visualizations mark the separation between the external undisturbed flow and the internal flow dominated by the dynamic stall vortex.[27] Of course, because of the slow shutter time of the camera (i.e., 1 ms), no small-scale vortex structures can be recognized in Fig. 3g. Instead, the streaklines form a large-scale rolling-up very similar to that of the numerical streamlines (Fig. 3b).

Poststall Vortex Shedding, α = 15-deg Downstroke

The preceding part of the dynamic stall process ends with the shedding of the dynamic stall vortex into the wake. The flowfield is then fully separated, and recent experimental[28] as well as numerical[20] investigations have shown the occurrence of secondary vortices either clockwise (starting close to the airfoil leading edge) or counterclockwise (starting from the trailing edge) during the downstroke part of the airfoil motion.

As an example of the kind of flowfield encountered during downstroke, the experimental and numerical results corresponding to a PIV recording taken at an incidence of 15-deg downstroke are shown in Fig. 4. The numerical results in the streamline plot of Fig. 4a show the development of two separated flow areas which have a structure similar to that of the measured field. The numerical vorticity contour plot (Fig. 4b) shows the shedding of a clockwise (from the leading edge) and a counterclockwise (from the trailing edge) vortex. This shedding of secondary vortices takes place alternatively. The numerical data and the experimental data are similar with regard to the vorticity distribution and structure. The counterclockwise vortex, however, is not visible on the experimental results because of data dropout. Again, the experimental results generally show a more complex spatial distribution than the numerical ones.

This kind of comparison can be done for all of the PIV pictures taken during downstroke, the flowfield being strongly different from one picture to the next. For example, Geissler et al.[21] report PIV and numerical results for three different incidences and show how the separated flowfield reduces from three distinct flow areas (at 23 deg) to two (at 15 deg; see Fig. 4) and finally to one (at 13 deg).

Another important point concerns the experimental results on the downstroke part of the airfoil motion: Unlike the upstroke, where the development of the dynamic stall vortex was seen to be reasonably reproducible in time and space from cycle to cycle, major differences in the overall flowfield structure were observed (for the exact same instantaneous incidence) on the six PIV and numerous visualization pictures recorded in successive periods, indicating a strong effect of nonreproducibility of the flow phenomena (Figs. 5a and 5b). This nonreproducibility effect already has been mentioned by several authors working on the dynamic stall problem. McAlister et al.[22] have shown that at least 50 cycles must be averaged to sufficiently remove the random part from their initial pressure measurements, and De Ruyck et al.[26] attributed, at some phases of the dynamic stall process, 10–50% of their measured turbulence intensity to these cycle-to-cycle variations. A more complete review is given in Ref. 12. An important consequence of this observation is that

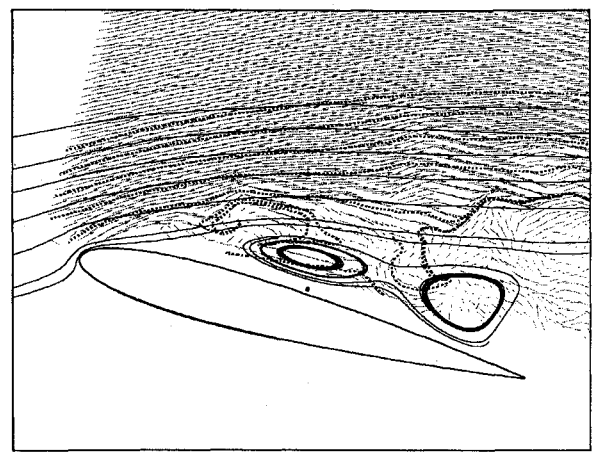

a) - - - -, PIV, α = 15 deg down and ——, calculations, α = 15 deg down

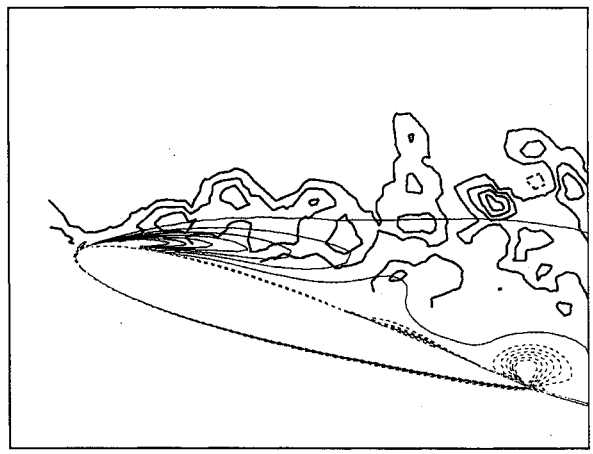

b) PIV. α = 15 deg down: ——, clockwise and - - - -, counterclockwise calculations; α = 15 deg down: ——, clockwise and – – –, counterclockwise

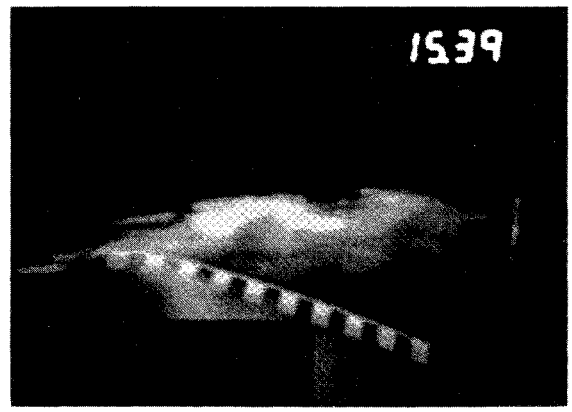

c) 15.39 deg < α < 14.98 deg

Fig. 4 Phase of poststall vortex shedding (downstroke motion): a) PIV velocity vector field and streamlines from calculations and PIV experiment, b) vorticity contours from calculations and PIV experiment, and c) visualization picture.

the standard experimental operating mode (phase averaging) used for LDA or pressure measurements should be employed carefully because it eliminates important instantaneous effects and includes these cycle-to-cycle variations when determining turbulence intensities. This effect of nonreproducibility also makes the comparison between experimental and numerical results particularly difficult or even irrelevant. The choice of the visualization picture is also complicated because the PIV and visualization recordings were not made at the same time.

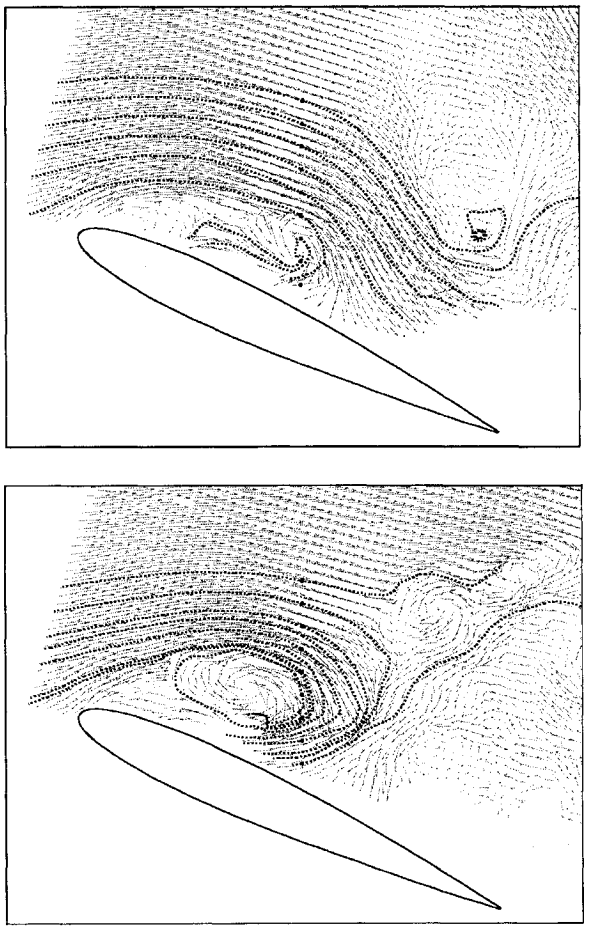

Fig. 5 Velocity vector fields and streamlines (dotted line) from two PIV records taken in successive oscillation periods of the airfoil at the same incidence of α = 24 deg downstroke.

Finally, comparison of Figs. 2 (α = 15-deg upstroke) and 4 (α = 15-deg downstroke) shows the strong hysteresis effect involved in the dynamic stall process.

Reattachment Process, $\alpha \leq$ 10-deg Downstroke

The last part of the dynamic stall process is the phase of reattachment. Because it is an unavoidable event following the phase of flow separation during downstroke, the reattachment has received little attention. However, it should be considered as a phase of primary importance because the lift- and pitching-moment loops are strongly dependent on it. A proper understanding of the reattachment process is therefore essential to improve the aerodynamic performances and damping characteristics (related to the stall flutter problem) of the airfoil.

Among the few articles dedicated to the reattachment phase, Niven and McD. Galbraith[29] analyzed the reattachment process of separated flows on a two-dimensional airfoil undergoing rampdown motions and gave important conclusions on the influence of airfoil geometry and reduced frequency on the location of the reattachment point. Ahmed and Chandrasekhara[30] studied the flowfield on a NACA 0012 airfoil pitching at a Reynolds number of 5.4×10^5 (close to the Reynolds number of the present investigations). They found that, contrary to the steady flow where reattachment is a sudden event, it occurs over a large range of angles of attack when the airfoil oscillates. In fact, the separated leading-edge shear layer begins to reattach as the static stall incidence is approached during downstroke, and the reattachment process is completed over the entire airfoil upper surface at a very low angle of attack. A complete description of this flowfield event (including the presence and role of a separation bubble and a suction peak in the pressure distribution) is also given in Ref. 30.

Figure 6 shows a comparison of experimental and numerical results during the reattachment phase ($\alpha \leq$ 10 deg). The reattachment

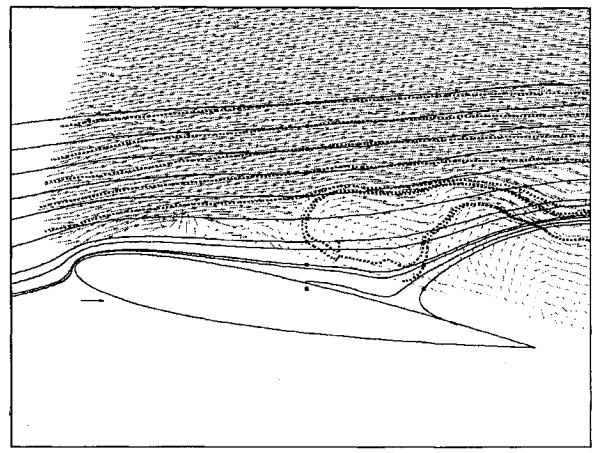

a) - - - -, PIV, α = 10 deg down and ——, calculations, α = 10 deg down

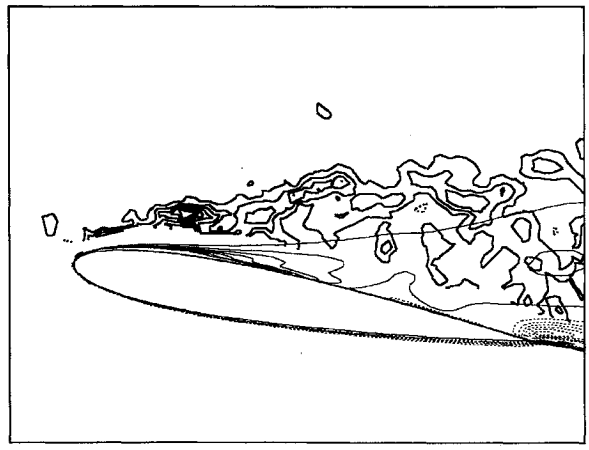

b) PIV. α = 10 deg down: ——, clockwise and - - - -, counterclockwise calculations; α = 10 deg down: ——, clockwise and – – –, counterclockwise

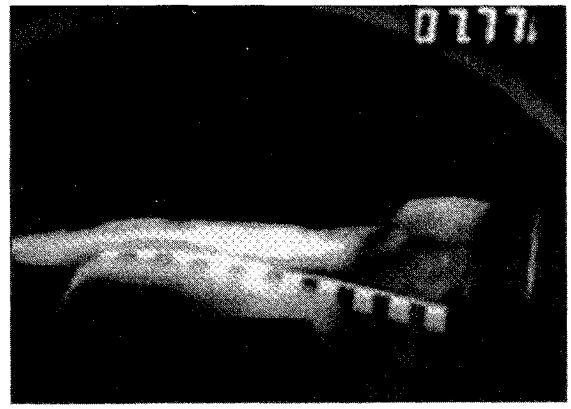

c) 7.77 deg < α < 7.48 deg

Fig. 6 Phase of reattachment (downstroke motion): a) PIV velocity vector field and streamlines from calculations and PIV experiment, b) vorticity contours from calculations and PIV experiment, and c) visualization picture.

process develops from front to rear. The streamlines shown in Fig. 6a are similar for both calculated and experimental data. However, in the numerical data, the reattachment process is considerably ahead of the experimental one. The same conclusion can be drawn from the vorticity results (Fig. 6b). To quantify the phase lead of the numerical data over the experimental data concerning the reattachment process, the visualization picture (Fig. 6c) was chosen to show a comparable spatial extent of the region of reattachment. The airfoil incidence corresponding to Fig. 6c (7.77 deg < α < 7.48 deg

downstroke) indicates a deviation of more than 2 deg in incidence between experiments and calculations. Once more, wind-tunnel effects may explain this difference.

Discussion

Laminar Flow Modeling and Transition

It is well known that, at the low Reynolds number of this experiment and for low incidences, a large region of laminar boundary layer develops on the airfoil suction side. For example, Refs. 31 and 32 contain boundary-layer information for the steady flow past a NACA 0012 airfoil at Reynolds numbers (4×10^5 and 3.75×10^5, respectively) very close to that of the present study. Similar results could be obtained in dynamic stall conditions[33]: there, the burst of a laminar separation bubble was interpreted as the trigger for leading-edge separation and dynamic stall onset. Hence, it is expected that the absence of laminar boundary-layer modelization may lead to some errors in the numerical results.[25]

This modelization is also highly desirable at high incidences (close to the incidence of dynamic stall onset) although the extent of the laminar flow region is very limited in the vicinity of the stagnation point. Indeed, in a recent numerical investigation, Currier and Fung[34] showed that the flowfield is very sensitive to the boundary-layer conditions at stall onset. For example, a variation of 0.1% in the location of the transition point can lead to great variations in lift values for incidences just prior to stall. Thus, taking the transition process into account is indispensable for obtaining better numerical results. Unfortunately, very little is known about the displacement of the transition point (or bubble) at dynamic stall conditions. The classic criteria used for steady flows (e.g., Michel's criterion) have been shown to be inoperative in unsteady flows (and also in some steady flow conditions).[35] However, a transition criterion valid for steady and unsteady flows could be derived very recently by Favier et al.[36] This criterion also could be extended to for-and-aft motions and to pitching motions with experimental conditions close to the present ones: Therefore, this criterion should be considered for implementation in numerical codes.

Turbulent Flow Modeling

An adequate turbulence model is necessary in most computational fluid dynamics (CFD) codes to correctly model the small-scale structures involved in the flowfield. In the case of an airfoil pitching under deep dynamic stall conditions, this requirement becomes indispensable because the strong nonlinear effects of the flow may transform these small-scale structures into large-scale ones that can dominate the flowfield.

Some recent publications have provided new insights into the influence of the turbulence model on the flowfield prediction. Srinivasan et al.[37] evaluated the ability of five widely used turbulence models to calculate the unsteady separated flowfield over a NACA 0012 airfoil pitching in dynamic stall conditions by using a Navier–Stokes code. As was already known, they showed that the Baldwin–Lomax model (the most commonly used in CFD codes) provides poor results if massive separation appears in the flow. Significant improvements over the Baldwin–Lomax model are obtained (with almost no additional computational cost) with another equilibrium model, the renormalization group model. To take into account the historical effects of the flow, so-called nonequilibrium models were tested: Johnson–King, Baldwin–Barth, and Spalart–Allmaras. Major differences were observed between these five turbulence models on the aerodynamic loadings, location of flow-reversal points, and instantaneous streamline patterns. In general, the best predictions have been obtained with these nonequilibrium models.

Similar studies were conducted by Rizzetta and Visbal[38] (comparison of Baldwin–Lomax and $k-\epsilon$ models) and Dindar and Kaynak[39] (comparison of Baldwin–Lomax, Cebeci–Smith, and Johnson–King models). The results also show that the nonequilibrium models better predict the dynamic stall process. Hence, the implementation into the present numerical code of one of these nonequilibrium models (the Johnson–King model) is under way.

Conclusion

The unsteady flowfield past a NACA 0012 airfoil pitching under deep dynamic stall conditions has been investigated in an open low-speed wind tunnel by means of PIV, laser-sheet visualizations, and Navier–Stokes calculations. Although velocity data were missing from some critical regions on the PIV pictures, examination of the experimental results has shown the occurrence of a thin reverse-flow layer on the airfoil upperside when the flow is attached, the presence of small-scale vortex structures even inside the dynamic stall vortex during the time of its formation, the strong nonreproducibility effect of the separated flowfield during downstroke, and the progressive reattachment from the leading to the trailing edge. The calculation of the out-of-plane vorticity contours from the PIV velocity fields also has allowed details of the structure and locations of the vortices involved in the flow phenomenon to be described.

The four main phases of the dynamic stall process (attached flow, dynamic stall vortex development, poststall vortex shedding, and reattachment) can be correctly reproduced by the calculations. However, improvements in the numerical study are needed. The presence of the wind-tunnel walls should be modeled as discrepancies appear between the incidences of experimental and numerical results. A laminar boundary-layer model combined with a powerful transition criterion should be implemented to take into account the existence of a leading-edge laminar separation bubble. Last, more-sophisticated turbulence models (nonequilibrium models) should be used. The PIV pictures also have clearly shown the strong aperiodicity of the flow phenomenon when massive flow separation occurs. Hence, to better understand the mechanisms involved in the dynamic stall process, the standard phase-averaging procedure should be used very carefully.

Acknowledgments

The authors thank H. J. Schäfer (ISL) for his support in organizing the cooperative measurements, A. Köneke (ISL) for his work on the visualization pictures, G. Koerber, F. Wietrich (ISL), and H. Seyb (DLR) for their help during the experimental measurements, B. Bretthauer (DLR) for his assistance during the phase of evaluation of the PIV records, and H. Vollmers (DLR) for the final representation of the velocity and vorticity results by means of the Comadi software tool.[40]

References

[1]Kramer, M., "Increase in the Maximum Lift of an Airfoil Due to a Sudden Increase in Its Effective Angle of Attack Resulting from a Gust," NACA TM 678, 1932.

[2]Carr, L. W., McAlister, K. W., and McCroskey, W. J., "Analysis of Dynamic Stall Based on Oscillating Airfoils Experiments," NASA TN D-8382, Jan. 1977.

[3]Geissler, W., Carr, L. W., and Cebeci, T., "Viscous/Inviscid Interaction Procedure for High Amplitude Oscillating Airfoil," *Proceedings of the 16th Congress of the International Council of the Aeronautical Sciences* (Jerusalem, Israel), 1988, pp. 766–778.

[4]Mehta, U. B., "Dynamic Stall of an Oscillating Airfoil," *Unsteady Aerodynamics* (Ottawa, ON, Canada), CP-227, AGARD, 1977, pp. 23.1–23.32.

[5]Geissler, W., "Numerical Investigation of Dynamic Stall on Oscillating Airfoil," *International Forum on Aeroelasticity and Structural Dynamics* (Aachen, Germany), 1991, pp. 85–93.

[6]McCroskey, W. J., "The Phenomenon of Dynamic Stall," NASA TM 81264, March 1981.

[7]Hussain, A. K. M. F., and Reynolds, W. C., "The Mechanics of an Organized Wave in Turbulent Shear Flow," *Journal of Fluid Mechanics*, Vol. 41, No. 2, 1970, pp. 241–264.

[8]Wernert, P., Koerber, G., and Wietrich, F., "LDA Measurements of the Unsteady Near Wake Behind an Airfoil Undergoing Transient and Periodic Pitching Motions," *Proceedings of the 6th International Symposium on Applications of Laser Techniques to Fluid Mechanics* (Lisbon, Portugal), 1992 (Paper 13.1 and ISL Rept. CO 215/92).

[9]Adrian, R. J., "Particle-Imaging Techniques for Experimental Fluid Mechanics," *Annual Review of Fluid Mechanics*, Vol. 23, 1991, pp. 261–304.

[10]Grant, I. (ed.), *Selected Papers on Particle Image Velocimetry*, SPIE Milestone Series No. 99, International Society for Optical Engineering, 1994.

[11]Wernert, P., Koerber, G., and Wietrich, F., "A New Experimental Apparatus for the Study of the Unsteady Flowfield Over an Airfoil in Pitching and Heaving Motions Using Laser Doppler Anemometry," *Proceedings of the European Forum on Wind-Tunnels and Wind-Tunnel Test Techniques* (Southampton, England, UK), 1992, pp. 45.1–45.10 (ISL-Rept. CO 229/92).

[12]Raffel, M., Kompenhans, J., and Wernert, P., "Investigation of the Unsteady Flow Velocity Field Above a NACA 0012 Airfoil Pitching Under

Deep Dynamic Stall Conditions," *Experiments in Fluids*, Vol. 19, 1995, pp. 103–111.

[13]Wernert, P., Köneke, A., Wietrich, F., and Koerber, G., "Visualisation du Phénomène de Décrochage Dynamique sur Profil Oscillant: Dispositif Expérimental, Prises de Vues, Mesure Précise de l'Incidence et Traitement d'Images," Inst. of Saint Louis, ISL-Rept. RT 505/95, Saint Louis, France, 1995.

[14]Kompenhans, J., Raffel, M., Vogt, A., and Fischer, M., "Aerodynamic Investigations in Low and High Speed Wind Tunnels by Means of Particle Image Velocimetry," *Proceedings of the 15th International Congress on Instrumentation in Aerospace Simulation Facilities*, Inst. of Saint Louis, France, 1993, pp. 46.1–46.5.

[15]Raffel, M., and Kompenhans, J., "Theoretical and Experimental Aspects of Image Shifting by Means of a Rotating Mirror System for Particle Image Velocimetry," *Measurement, Science and Technology*, Vol. 6, June 1995, pp. 795–808.

[16]Raffel, M., Leitl, B., and Kompenhans, J., "Data Validation for Particle Image Velocimetry," *Laser Techniques and Applications in Fluid Mechanics, Proceedings of the 6th International Symposium on Applications of Laser Techniques to Fluid Mechanics* (Lisbon, Portugal), Springer–Verlag, Berlin, 1992, pp. 210–226.

[17]Beam, R., and Warming, R. F., "An Implicit Finite Difference Algorithm for Hyperbolic Systems in Conservative Law Form," *Journal of Computational Physics*, Vol. 22, Sept. 1976, pp. 87–110.

[18]Geissler, W., "Instationäres Navier-Stokes-Verfahren für beschleunigt bewegte Profile mit Ablösung," DLR, German Aerospace Research Establishment, DLR-FB 92-03, Göttingen, Germany, Jan. 1992, pp. 1–68.

[19]Baldwin, B. S., and Lomax, H., "Thin Layer Approximation and Algebraic Model for Separated Turbulent Flows," AIAA Paper 78-257, Jan. 1978.

[20]Geissler, W., and Vollmers, H., "Unsteady Separated Flows on Rotor-Airfoil," *Proceedings of the 18th European Rotorcraft Forum* (Avignon, France), 1992, pp. 79.1–79.12.

[21]Geissler, W., Kompenhans, J., Raffel, M., Vollmers, H., and Wernert, P., "Numerical and Experimental Investigations of Unsteady Flows Under Deep Dynamic Stall Conditions," *Proceedings of the 20th European Rotorcraft Forum* (Amsterdam, The Netherlands), 1994, pp. 22.1–22.19.

[22]McAlister, K. W., Carr, L. W., and McCroskey, W. J., "Dynamic Stall Experiments on the NACA 0012 Airfoil," NASA TP-1100, Jan. 1978.

[23]Tuncer, I. H., Wu, J. C., and Wang, C. M., "Theoretical and Numerical Studies of Oscillating Airfoils," *AIAA Journal*, Vol. 28, No. 9, 1990, pp. 1615–1624.

[24]Rae, W. H., and Pope, A., *Low-Speed Wind Tunnel Testing*, 2nd ed., Wiley, New York, 1984, Chap. 6.

[25]Telionis, D. P., *Unsteady Viscous Flows*, Springer Series in Computational Physics, Springer–Verlag, Berlin, 1981, pp. 224–225.

[26]De Ruyck J., Hazarika, B., and Hirsch, C., "Measurements of Velocity Profiles and Reynolds Stresses on an Oscillating Airfoil," *Unsteady Aerodynamic Phenomena in Turbomachines* (Luxembourg), CP-468, AGARD, 1989, pp. 23.1–23.15.

[27]Wernert, P., Koerber, G., Wietrich, F., Raffel, M., and Kompenhans, J., "Experimental Study of the Dynamic Stall Process on a Pitching Airfoil by Means of PIV Measurements and Laser-Sheet Measurements," *Proceedings of the 7th International Symposium on Applications of Laser Techniques to Fluid Mechanics* (Lisbon, Portugal), 1994, (Paper 38.1 and ISL-Rept. PU 315/94).

[28]Leishman, J. G., "Dynamic Stall Experiments on the NACA 23012 Aerofoil," *Experiments in Fluids*, Vol. 9, 1990, pp. 49–58.

[29]Niven, A. J., and McD. Galbraith, R. A., "Experiments on the Establishment of Fully Attached Aerofoil Flow from the Fully Stalled Condition During Ramp-Down Motions," *Proceedings of the 17th Congress of the International Council of Aeronautical Sciences* (Stockholm, Sweden), 1990, pp. 653–662.

[30]Ahmed, S., and Chandrasekhara, M. S., "Reattachment Studies of an Oscillating Airfoil Dynamic Stall Flowfield," *AIAA Journal*, Vol. 32, No. 5, 1994, pp. 1006–1012.

[31]Favier, D., "Aérodynamique Subsonique Instationnaire d'un Profil d'Aile Soumis à des Variations de Vitesse et d'Incidence," Ph.D. Thesis, Dept. of Unsteady Aerodynamics, Univ. of Aix Marseille II, Aix Marseille, France, Oct. 1980.

[32]Gartenburg, E., Roberts, S., and McRee, G. J., "Infrared Imaging and Tuft Studies of Boundary Layer Flow Regimes on a NACA 0012 Airfoil," *Proceedings of the 13th International Congress on Instrumentation in Aerospace Simulation Facilities* (Göttingen, Germany), 1989, pp. 168–178.

[33]Chandrasekhara, M. S., and Ahmed, S., "Laser Velocimetry Measurements of Oscillating Airfoil Dynamic Stall Flow Field," AIAA Paper 91-1799, June 1991.

[34]Currier, J. M., and Fung, K. Y., "Analysis of the Onset of Dynamic Stall," *AIAA Journal*, Vol. 30, No. 10, 1992, pp. 2469–2477.

[35]Cebeci, T., and Carr, L. W., "Calculation of Boundary Layers of Oscillating Airfoils," NASA TM-85943, May 1984.

[36]Favier, D., Maresca, M., Renon, P., and Autric, J. M., "Unsteady Boundary Layer Measurements on Oscillating Models Using an Optical Fibre LDA Technique," *Proceedings of the 6th International Symposium on Application of Laser Techniques to Fluid Mechanics* (Lisbon, Portugal), Paper 13.4, 1992.

[37]Srinivasan, G. R., Ekaterinaris, J. A., and McCroskey, W. J., "Dynamic Stall of an Oscillating Wing; Part 1: Evaluation of Turbulence Model," AIAA Paper 93-3403, Aug. 1993.

[38]Rizzetta, D. P., and Visbal, M. R., "Comparative Numerical Study of Two Turbulence Models for Airfoil Static and Dynamic Stall," *AIAA Journal*, Vol. 31, No. 4, 1993, pp. 784–786.

[39]Dindar, M., and Kaynak, U., "Effect of Turbulence Modeling on Dynamic Stall of a NACA 0012 Airfoil," AIAA Paper 92-0027, Jan. 1992.

[40]Vollmers, H., "Diagnostic and Visualization Tools for Flow Fields," *Proceedings of the 26th International Symposium on Automotive Technology and Automation* (Aachen, Germany), 1993 (Paper 93EM076).